Single-Crystal 9,10-Diphenylanthracene Nanoribbons and Nanorods

Xiujuan Zhang,[†,‡] Guodong Yuan,[‡] Quansong Li,[‡] Bo Wang,[§] Xiaohong Zhang,*[,§] Ruiqin Zhang,[‡] Jack C. Chang,[†,‡] Chun-sing Lee,[‡] and Shuit-tong Lee*[,‡]

Functional Nano & Soft Materials Laboratory (FUNSOM), Soochow University, Suzhou, Jiangsu 215123, China, Center of Super-Diamond and Advanced Films (COSDAF) and Department of Physics and Materials Science, City University of Hong Kong, Hong Kong SAR, China, and Nano-organic Photoelectronic Laboratory and Laboratory of Organic Optoelectronic Functional Materials and Molecular Engineering, Technical Institute of Physics and Chemistry, Chinese Academy of Sciences, Beijing 100101, China

Received April 7, 2008. Revised Manuscript Received September 18, 2008

Single-crystal 9,10-diphenylanthracene (DPA) nanoribbons and nanorods with uniform sizes and shapes were synthesized via a simple surfactant-assisted self-assembly process. The shape of the as-prepared nanostructures can be readily controlled by varying the solubility of DPA in the preparation solution. A growth mechanism was proposed for the formation of different morphological structures. Crystal structure analysis demonstrated that the overlap between the two phenyl groups at the opposite positions of the anthracene backbone forms effective intermolecular linking for crystal growth, in good agreement with prediction from quantum mechanical calculations. Electronic and optical properties of the as-prepared nanostructures are investigated.

Introduction

Recently, small molecular organic semiconductor nanostructures have attracted intense attention as they can offer tunable electronic and optical properties via molecular design, greater variety, and physical flexibility.[1−19] Morphology control of organic nanostructures is the current focus due to the need and interest for tuning optical and electronic properties.[20−23] For example, our group has fabricated uniformly shaped nanoribbons, nanotubes, and nanowires from the same organic compound and observed concurrent changes in shapes and optical properties.[24] Yao et al. reported tunable emission from organic nanostructures via size control of nanostructures.[25,26] Nakanishi et al. reported that emission of organic nanocrystals was strongly affected by surface characteristics.[27] Clearly, it is of practical interest to obtain organic nanostructures with controlled morphology, including shape, size, and surface. In this work, we study the nanostructures of 9,10-diphenylanthracene (DPA), which has two phenyl groups attached at the opposite (9,10)-positions of the anthracene backbone as shown in Scheme 1. DPA is an important functional molecule with high fluorescence

* Corresponding authors. Fax: +852-27844696 (S.-t.L.), +86-10-62554670 (X.Z.). E-mail: apannale@cityu.edu.hk (S.-t.L.), xhzhang@mail.ipc.ac.cn(X.Z.). Tel: +86-10-82543510(X.Z.).

[†] Soochow University.

[‡] City University of Hong Kong.

[§] Chinese Academy of Sciences.

(1) Escosura, A.; De, la; Martinez-Diaz, M. V.; Thordarson, P.; Rowan, A. E.; Nolte, R. J. M.; Torres, T. *J. Am. Chem. Soc.* **2003**, *125*, 12300.
(2) Che, Y.; Datar, A.; Balakrishnan, K.; Zang, L. *J. Am. Chem. Soc.* **2007**, *129*, 7234.
(3) Nguyen, T. Q.; Martel, R.; Avouris, P.; Bushey, M.; Nuckolls, C.; Brus, L. E. *J. Am. Chem. Soc.* **2004**, *126*, 5234.
(4) Liu, H. B.; Li, Y. L.; Xiao, S. Q.; Gan, H. Y.; Jiu, T. G.; Li, H. M.; Jiang, L.; Zhu, D. B.; Yu, D. P.; Xiang, B. Y.; Chen, F. *J. Am. Chem. Soc.* **2003**, *125*, 10794.
(5) Fu, H. B.; Xiao, D. B.; Yao, J. N.; Yang, G. Q. *Angew. Chem., Int. Ed.* **2003**, *42*, 2883.
(6) Hu, J. S.; Guo, Y. G.; Liang, H. P.; Wan, L. J.; Jiang, L. *J. Am. Chem. Soc.* **2005**, *127*, 17090.
(7) Zhang, X. J.; Zhang, X. H.; Shi, W. S.; Meng, X. M.; Lee, C. S.; Lee, S. T. *Angew. Chem., Int. Ed.* **2007**, *46*, 1525.
(8) Briseno, A. L.; Mannsfeld, S. C. B.; Reese, C.; Hancock, J. M.; Xiong, Y.; Jenekhe, S. A.; Bao, Z.; Xia, Y. *Nano Lett.* **2007**, *7*, 2847.
(9) Tang, Q.; Li, H.; Liu, Y.; Hu, W. *J. Am. Chem. Soc.* **2006**, *128*, 14634.
(10) Liu, H.; Zhao, Q.; Li, Y.; Liu, Y.; Lu, F.; Zhuang, J.; Wang, S.; Jiang, L.; Zhu, D.; Yu, D.; Chi, L. *J. Am. Chem. Soc.* **2005**, *127*, 1120.
(11) Schwab, A. D.; Smith, D. E.; Bond-Watts, B.; Johnston, D. E.; Hone, J.; Johnson, A. T.; de Paula, J. C.; Smith, W. F. *Nano Lett.* **2004**, *4*, 1261.
(12) Shimizu, L. S.; Hughes, A. D.; Smith, M. D.; Davis, M. J.; Zhang, B. P.; Loye, H. Z.; Shimizu, K. D. *J. Am. Chem. Soc.* **2003**, *125*, 14972.
(13) Herrikhuyzen, J. van.; Syamakumari, A.; Schenning, A. P. H. J.; Meijer, E. W. *J. Am. Chem. Soc.* **2004**, *126*, 10021.
(14) An, B. K.; Lee, D. S.; Lee, J. S.; Park, Y. S.; Song, H. S.; Park, S. Y. *J. Am. Chem. Soc.* **2004**, *126*, 10232.
(15) Harada, R.; Matsuda, Y.; Okawa, H.; Kojima, T. *Angew. Chem., Int. Ed.* **2004**, *43*, 1825.
(16) Lee, H. Y.; Nam, S. R.; Hong, J. I. *J. Am. Chem. Soc.* **2007**, *129*, 1040.
(17) Nafady, A.; Bond, A. M.; Bilyk, A.; Harris, A. R.; Bhatt, A. I.; O'Mullane, A. P.; Marco, R. D. *J. Am. Chem. Soc.* **2007**, *129*, 2369.
(18) Yoon, S.; Miller, E. W.; He, Q.; Do, P. H.; Chang, C. J. *Angew. Chem., Int. Ed.* **2007**, *46*, 6658.
(19) Barrett, C.; Iacopino, D.; O'Carroll, D.; Marzi, G. D.; Tanner, D. A.; Quinn, A. J.; Redmond, G. *Chem. Mater.* **2007**, *19*, 338.
(20) Zhang, X. J.; Zhang, X. H.; Meng, X. M.; Shi, W. S.; Lee, C. S.; Lee, S. T. *J. Phys. Chem. B* **2005**, *109*, 18777.
(21) Li, D.; Kaner, R. B. *J. Am. Chem. Soc.* **2006**, *128*, 968.
(22) Wang, Y. B.; Fu, H. B.; Peng, A. D.; Zhao, Y. S.; Ma, J. S.; Ma, Y.; Yao, J. N. *Chem. Commun.* **2007**, 1623.
(23) Yamamoto, Y.; Fukushima, T.; Suna, Y.; Ishii, N.; Saeki, A.; Seki, S.; Tagawa, S.; Taniguchi, M.; Aida, T. *Science* **2006**, *314*, 1761.
(24) Zhang, X. J.; Zhang, X. H.; Zou, K.; Lee, C. S.; Lee, S. T. *J. Am. Chem. Soc.* **2007**, *129*, 3527.
(25) Kang, L.; Wang, Z.; Cao, Z.; Ma, Y.; Fu, H.; Yao, J. *J. Am. Chem. Soc.* **2007**, *129*, 7305.
(26) Zhao, Y. S.; Xiao, D.; Yang, W.; Peng, A.; Yao, J. *Chem. Mater.* **2006**, *18*, 2302.
(27) Kwon, E.; Chung, H. R.; Araki, Y.; Kasai, H.; Oikawa, H.; Ito, O.; Nakanishi, H. *Chem. Phys. Lett.* **2007**, *441*, 106.

10.1021/cm801896r CCC: $40.75
Published on Web 10/23/2008

Scheme 1. Chemical Structure (a) and Energy-Optimized Configuration (b) of a Single 9,10-Diphenylanthracene (DPA) Molecule

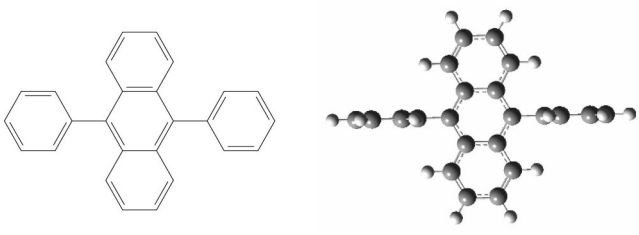

(a) (b)

efficiency and is widely used in organic optoelectronics.[28−31] We report the synthesis of single-crystalline DPA semi-one-dimensional nanoribbons (semi-1-D) and one-dimensional (1-D) nanorods with highly uniform sizes and shapes by tuning the solubility of DPA in the preparation solution with the assistance of surfactant. A possible growth mechanism is proposed. Theoretical calculation and X-ray diffraction (XRD) analysis were performed, and showed that the overlap between the two phenyl groups attached at the opposite positions of the anthracene backbone forms effective intermolecular $\pi-\pi$ linking in the crystals. Field-effect transistors were fabricated to explore the electronic properties, and optical study showed nanoribbons and nanorods have similar photoluminescence spectra.

Experimental Section

Materials. 9,10-Diphenylanthracene and cetyltrimethyl ammonium bromide (CTAB) were purchased from Aldrich Chemical Co. High-purity water (resistivity = 18.2 MΩ cm) was produced with a Milli-Q apparatus (Millipore) and filtered using an inorganic membrane with a pore size of 0.02 μm (Whatman International, Ltd.) just before use. Tetrahydrofuran (THF) was obtained from Beijing Chemical Agent and used without further purification.

Preparation. In a typical synthesis, 0.1−1 mL of 2×10^{-3} M DPA/THF solution was injected respectively into 5 mL of surfactant/water (CTAB/water, 0.5 mM) solution at room temperature under vigorous stirring. After stirring for 3 min, the sample was left standing for about 2 h for stabilization.

Characterization. For scanning electron microscopic (SEM) studies, a few drops of the sample were placed onto silicon substrates, and the solvent was left to evaporate. The samples were then examined with a field emission SEM (Philips XL 30 FEG) operated at an accelerating voltage of 5 kV. To minimize sample charging, an ultrathin layer of Au was deposited onto the samples before SEM examination. Samples for transmission electron microscopy (TEM) were prepared by placing a drop of suspension on a copper grid coated with carbon film and then dried in air for a few hours before observation. The TEM study was performed in a Philips CM20 TEM operated at an accelerating voltage of 200 kV. XRD spectra were recorded with a Japan Mac Science M18AHF X-ray diffractometer using Cu Kα radiation ($\lambda = 1.54050$ Å). For device fabrication, patterned Ti (100 nm) and Au (25 nm) electrodes were fabricated on a SiO_2 (300 nm thick)/Si wafer using UV photolithography technique. Current−voltage ($I-V$) characteristics of FET were performed by using a two-probe configuration under ambient conditions.

Computational Method. The quantum mechanical calculation was conducted by using the self-consistent-charge density-functional tight-binding (SCC-DFTB) method [32,33] from an energetic standpoint. The DFTB method is derived from density functional theory (DFT) as a second-order expansion of the DFT total energy functional with respect to the charge-density fluctuations around a given reference density. The configuration of DPA in Scheme 1 was optimized from the corresponding minimum energy process using the B3LYP/6-31G* method in Gaussian 98.

Results and Discussion

Figure 1 shows typical scanning electron microscopy (SEM) images of the resulting nanostructures with different morphologies obtained by tuning the solubility of DPA in the preparation solution via varying the added volumes of DPA/THF solutions. When 0.1 mL of DPA/THF solution was injected into 5 mL of CTAB/H_2O solution, ribbon-like structures with smooth surfaces were obtained (Figure 1a). The ribbons had a width of about 500 nm, a thickness of 20−30 nm, and a length up to 20 μm. When the volume of DPA/THF was increased to 0.3 mL, the dimensions of the nanoribbons (Figure 1b) were substantially increased. The resulting nanoribbons had an average width of 5 μm and a thickness of 70−80 nm. As the volume of DPA/THF was increased to 0.4 mL, some small 1-D nanostructures (Figure 1c) emerged among the nanoribbons. When the volume of DPA/THF was further increased to 0.5 and 1 mL, the dimension of the nanostructures continued to increase (Figure 1d,e). They gradually grew into nanorods with a width of about 450 nm and a length of 4−5 μm as shown in Figure 1e (see Supporting Information Part S1). It can be seen that with more DPA/THF added in the preparation solution, the solubility of DPA in the solution increases and the shape of the products changed from nanoribbons to nanorods accordingly. Figure 2a,b shows typical transmission electron microscopy (TEM) images of a single nanoribbon and the nanorods, respectively. The TEM results basically confirm the morphology observed with SEM. The insets in Figure 2 depict the select-area electron diffraction (SAED) patterns of the corresponding nanostructures. Identical SAED patterns were obtained along the entire length of the nanoribbon/rods, showing the uniform single-crystal nature of the nanostructures. Structures of the nanoribbons and nanorods were also investigated by XRD analysis (Figure 3). The sharp peaks in the XRD spectra further confirm the nanostructures to be highly crystalline. It can be seen that the XRD spectra of nanoribbons and nanorods are essentially the same and similar to that of the starting powder materials. Analysis shows that the crystal structure is monoclinic with lattice

(28) Norifusa, S.; Sang, C. J.; Masayoshi, H.; Kimihisa, Y. *J. Am. Chem. Soc.* **2003**, *125*, 8104.
(29) Balaganesan, B.; Shen, W. J.; Chen, C. H. *Tetrahedron Lett.* **2003**, *44*, 5747.
(30) Raghunath, P.; Reddy, M. A.; Gouri, C.; Bhanuprakash, K.; Rao, V. J. *J. Phys. Chem. A* **2006**, *110*, 1152.
(31) Tripathi, A. K.; Heinrich, M.; Siegrist, T.; Pflaum, J. *Adv. Mater.* **2007**, *19*, 2097.
(32) Porezag, D.; Frauenheim, Th.; Köhler, Th.; Seifert, G.; Kaschner, R. *Phys. Rev. B* **1995**, *51*, 12947.
(33) Niehaus, T. A.; Suhai, S.; Sala, F. D.; Lugli, P.; Elstner, M.; Seifert, G.; Frauenheim, Th. *Phys. Rev. B* **2001**, *63*, 085108.

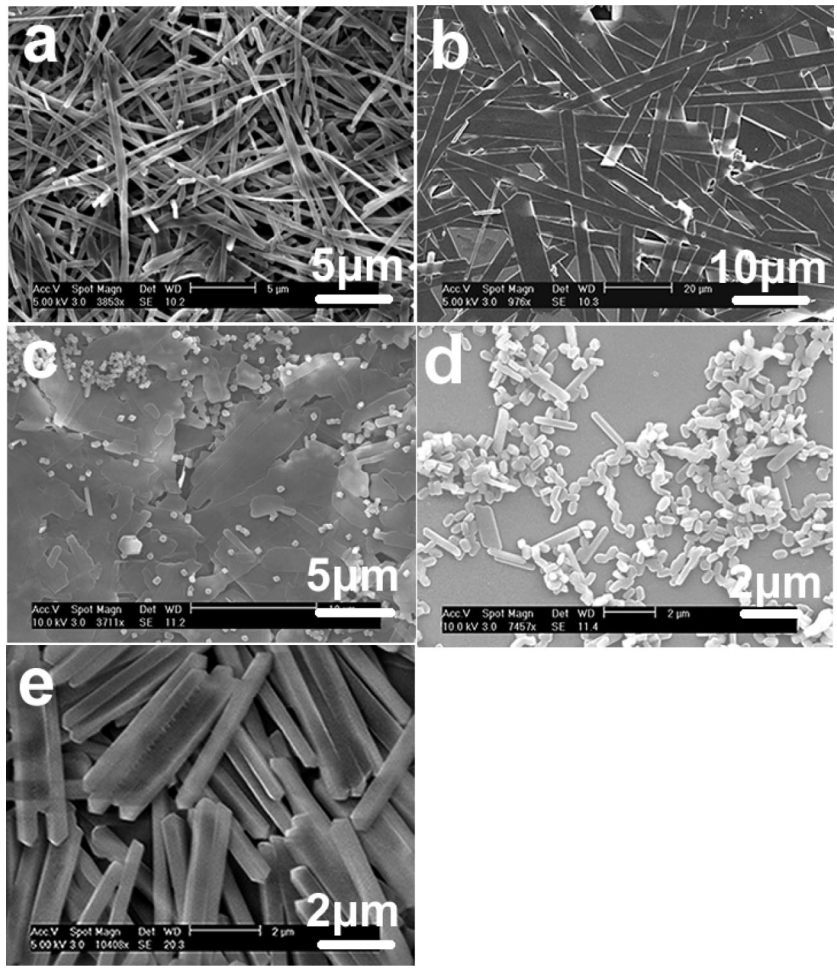

Figure 1. SEM images of DPA nanostructures prepared by injecting (a) 0.1; (b) 0.3; (c) 0.4; (d) 0.5; and (e) 1 mL of 2×10^{-3} M DAP/THF solution into 5 mL of 1 mM CTAB aqueous solution.

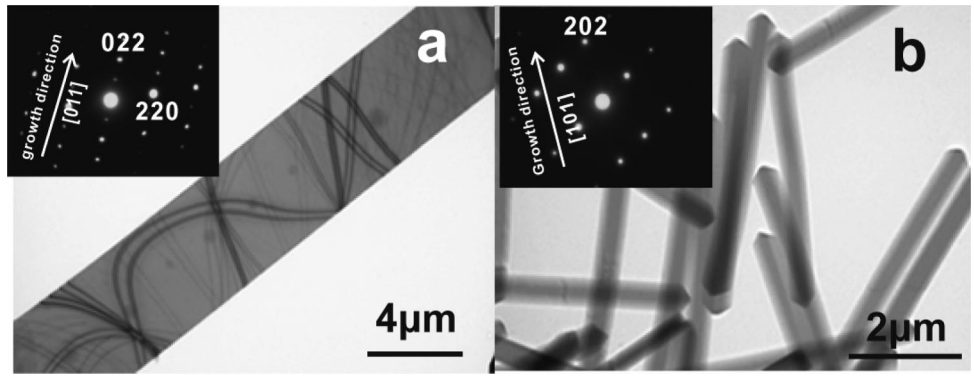

Figure 2. TEM images of DPA nanostructures: (a) nanoribbon, (b) nanorods. Inset in each image is the corresponding selected area electron diffraction (SAED) pattern.

parameters of $a = 10.70$ Å, $b = 13.57$ Å, $c = 12.29$ Å, $\alpha = 90°$, $\beta = 90.65°$, $\gamma = 90°$, and space group $C2/c$ [31,34,35] (see Supporting Information Part S2). It should be noted that the relative intensity of the characteristic (022) and (202) peaks of nanoribbons and nanorods remarkably increased as compared to those of the DPA powder materials. With the lattice parameters determined from the XRD results, discrete diffraction spots in Figure 2 were indexed accordingly. It is shown that the length direction of the nanoribbon is along the [011] direction while the longitudinal axis of the nanorod is parallel to the [101] direction. Figure 3b shows the structural projection of the crystallographic (*ac*)- and (*bc*)-planes of DPA, illustrating the molecular packing mode of DPA molecules in the crystal as determined from X-ray structure analysis. It shows that the contact between the two phenyl groups at the side of adjacent molecules forms effective intermolecular $\pi-\pi$ linking in the crystals, which is in good agreement with the prediction from quantum

(34) Dong, C. *J. Appl. Crystallogr.* **1999**, *32*, 838.
(35) Langer, V.; Becker, H. D. *Z. Kristallogr.* **1992**, *199*, 313.
(36) Xiong, Y.; Xia, Y. *Adv. Mater.* **2007**, *19*, 3385.

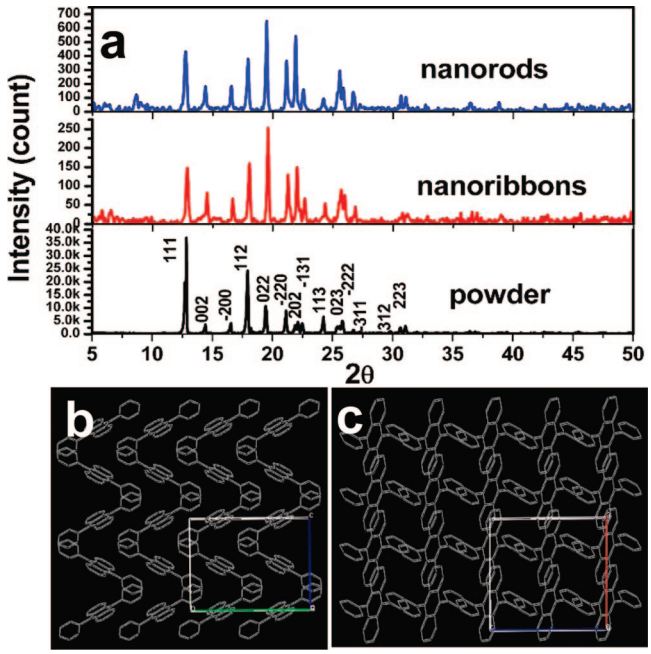

Figure 3. (a) XRD patterns of DPA powders (blank), nanoribbons (red), and nanorods (blue); parts b and c show structural projection of the crystallographic (*ac*)- and (*bc*)-planes of DPA as determined from powder X-ray diffraction.

mechanical calculation predictions (Figure 4). Structural optimizations and binding energies were calculated using the SCC-DFTB method. As shown in Figure 4a, a DPA molecule contains five benzene rings, which can be classified into three types, labeled A, B, and C. In the optimized structures, type A and C rings are in one plane, while type B rings are nearly perpendicular to this plane. Here, we consider three different $\pi-\pi$ stacking models of DPA chains with quantum mechanical calculations: AA overlap, BB overlap, and AB overlap are shown respectively in parts b, c, and d of Figure 4. In the case of AB stacking, the two benzene rings are not parallel, and the dihedral angel between them is about 20°; therefore, the distance between them is substantially increased resulting in a much weaker interaction. Figure 5a shows the optimized packing of eight molecules in AA, BB, and AB stacking. To evaluate the energy stability of these chains, we calculated their binding energies (BEs) per numbers of DPA molecules as shown in Figure 5b, which is defined as the energy necessary to dissociate the nanostructures into isolated DPA molecules, $E_{BE} = \{E[(PDA)_n] - nE(PDA)\}/n$, where n is the number of DPA units, up to 16 in our models. It is clear that the chain with BB stacking is energetically more favorable than those with AA and AB stacking, with the sequence being BB < AA < AB. The highest stability of the chain with BB stacking is most likely associated with the smallest steric hindrance of the BB stacking.

To elucidate the formation processes of the different nanostructures, we performed additional experiments. First, to verify the role of solubility change in nanoribbons preparation, we kept all other parameters constant but used either one-half the volume of water (poor solvent of DPA in the experiment) or twice the volume of THF (good solvent of DPA). The obtained products all changed from semi-1-D nanoribbons to 1-D nanorods (see Supporting Information Part S3). The same results were observed in the preparation of nanorods. Semi-1-D nanoribbons were obtained if we increased/decreased the volume of poor/good solvent, respectively, with all other parameters unchanged. It suggests that solubility of DPA plays an important role in the formation process of different morphologies. Second, by keeping all other parameters unchanged, we prepared the sample without surfactant and obtained, besides some irregular products, ribbon-like nanostructures as shown in Supporting Information Part S4. It suggests that DPA molecules tend to form ribbon-like structures due to its inherent anisotropic growth nature, even without the assistance of surfactant. However, without surfactant, no 1-D nanorods were formed in the products regardless of the solubility change. It demonstrated that surfactant is essential for the formation of 1-D nanorods and not only is the morphology control achieved by solubility change of DPA itself but also it is important to be assisted by surfactant. Finally, besides the cationic surfactant CTAB, we also studied the growth of DPA nanostructures using other surfactants, such as sodium dodecyl sulfate (SDS, an anionic surfactant) and Pluronic (a neutral surfactant), and obtained similar results with morphology changes.

These observations provide insights into the mechanisms of morphological changes from nanoribbons to nanorods. When a small volume of DPA/THF was added to the system, the solubility of DPA in the mixed solution was low. The crystals tend to take up a ribbon-like shape due to its inherently anisotropic growth nature.[37] Surfactants would attach to the seeds through hydrophobic interactions between the alkyl chains and the DPA molecules, forming a protective layer to block further aggregation. With increasing volume of DPA/THF and other parameters kept constant, the solubility of DPA in the mixed solution increases. Change of solvent composition (solubility) may have the following possible effects in the crystal growth process. First, the change of solubility of DPA in the preparation system would have a great impact on the supersaturation profile during the nucleation process and then subsequent growth kinetics in different directions, which may possibly change the shape of the crystals. Second, change of solvent composition may also modify the relative order of surface energy by preferential adsorption/desorption of surfactant on specific crystal surfaces. It is known that the crystal growth rate is exponentially related to surface energy, when surfactants preferentially stabilize a certain surface by "selective adsorption", the growth rate difference between different crystallographic directions would be accentuated,[38−40] resulting in the final morphology change. In this case, surfactant not only may serve as the protecting agent but also as "crystal-habit modifier" during crystal growth, inducing elongation along

(37) Cross, M. C.; Hohenberg, P. C. *Rev. Mod. Phys.* **1993**, *65*, 851.
(38) Boer, R. W. I. de.; Gershenson, M. E.; Morpurgo, A. F.; Podzorov, V. *Phys. Status Solidi A* **2004**, *201*, 1302.
(39) Zhang, Z.; Zhong, Z.; Liu, S.; Li, D.; Han, M. *Angew. Chem., Int. Ed.* **2005**, *44*, 3466.
(40) Ghezelbash, A.; Sigman, M. B., Jr.; Korgel, B. A. *Nano Lett.* **2004**, *4*, 537.

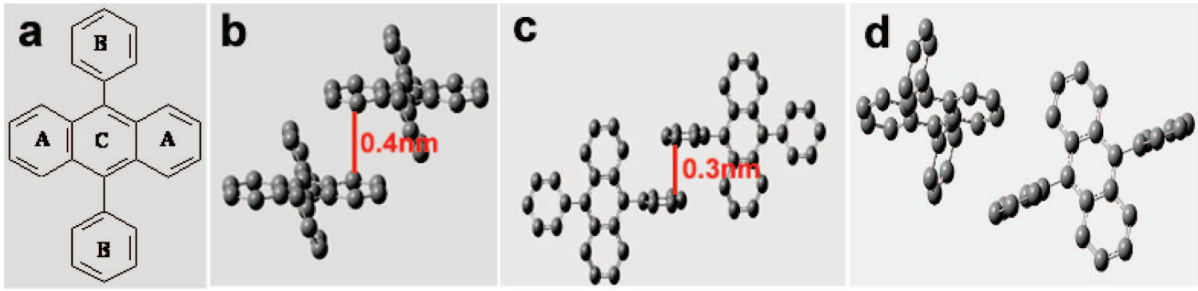

Figure 4. Molecular structure of DPA (a) showing three different types of rings; schematics showing the three stacking modes of DPA with (b) AA overlap; (c) BB overlap; and (d) AB overlap.

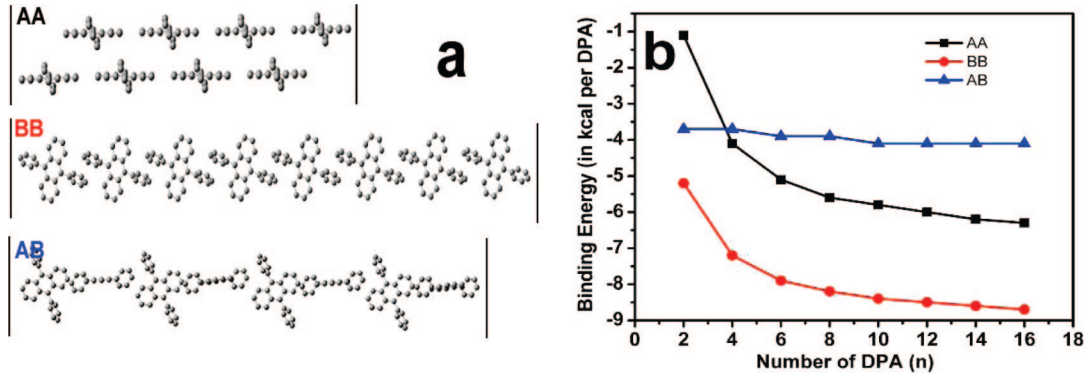

Figure 5. (a) Models of DPA nanowires induced by three different modes of directional $\pi-\pi$ stacking with AA, BB, or AB overlap; (b) binding energies per DPA unit as a function of the chain size for the three stacking modes.

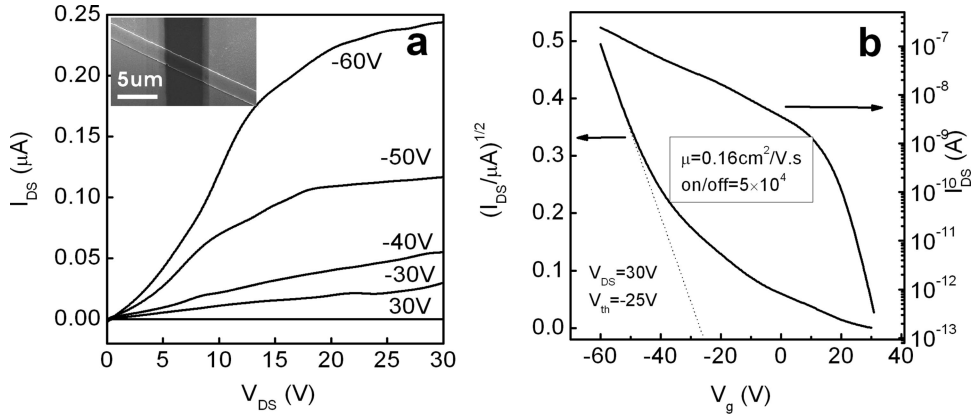

Figure 6. Output (a) and transfer characteristics (b) of a DPA nanoribbon FET.

specific axes.[41] Another possible reason for 1-D nanorod formation is that surfactants would readily self-assemble into rod-like or wire-like micelles in water depending on the concentration and the presence of other additives.[42,43] Such structures would serve as the template for molecular aggregations. However, the role of surfactants is still not totally clear, despite the large amount of work conducted on the soft templates in inorganic systems.[44−47] The current prevailing understanding supports that these surfactants might not behave as a physical template but rather as growth directing adsorbates on surfaces.[48,49]

We also investigated the electronic properties of the nanostructures by fabricating and characterizing the field effect transistor (FET) device from a single DPA nanoribbon on a Si/SiO_2 (300 nm) substrate. Typical output and transfer characteristics of the FET are shown in Figure 6. The inset in Figure 6a shows a representative SEM image of a Ti/Au top-contact device constructed from a single DPA nanoribbon. The FET exhibits p-type characteristics, and the hole mobility of the DPA nanoribbon can be estimated from $I_{DS} = [WC/(2L)]\mu(V_g - V_{th})^2$, where W and L are the width and effective contact length of the DPA nanoribbon and C is the capacitance, respectively. The capacitance is given by $C =$

(41) Jun, Y. W.; Choi, J. S.; Cheon, J. *Angew. Chem., Int. Ed.* **2006**, *45*, 3414.
(42) Shikata, T.; Hirata, H.; Kotaka, T. *Langmuir* **1988**, *4*, 354.
(43) Lianos, P.; Lang, J.; Strazielle, C.; Zana, R. *J. Phys. Chem.* **1982**, *86*, 1019.
(44) Jana, N. R.; Murphy, C. J. *Chem. Commun.* **2001**, 617.
(45) Murphy, C. J.; Jana, N. R. *Adv. Mater.* **2002**, *14*, 80.
(46) Ghezelbash, A.; Korgel, B. A. *Langmuir* **2005**, *21*, 9451.
(47) Sundar, V. C.; Zaumsei, J.; Podzorov, V.; Menard, E.; Willett, R. L.; Someya, T.; Gershenson, M. E.; Rogers, J. A. *Science* **2004**, *303*, 1644.
(48) Lee, S. M.; Jun, Y. W.; Cho, S. N.; Cheon, J. *J. Am. Chem. Soc.* **2002**, *124*, 11244.
(49) Tao, A. R.; Habas, S.; Yang, P. *Small* **2008**, *4*, 310.

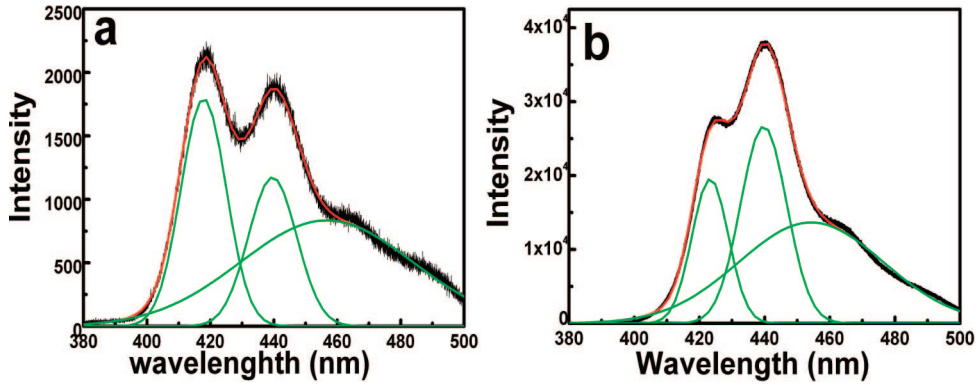

Figure 7. Photoluminescence spectra of nanoribbons (a) and nanorods (b).

$\varepsilon_{SiO_2}\varepsilon_0/h$, where ε_{SiO_2} is the dielectric constant of the gate SiO_2 and h is its thickness. The average channel width-to-length (W/L) ratio of the nanoribbon in the FET device is about 0.29. The analysis led to $C = 10^{-8}$ F/cm^2. The slope of the $I_{DS}^{1/2}-V_g$ curve in Figure 6b should be $(WC\mu/2L)^{1/2}$, and on the basis of this the hole mobility (μ) was derived to be about 0.16 cm^2 V^{-1} s^{-1} at $V_{DS} = 30$ V from the linear part of the saturation region as shown in Figure 6b. The threshold voltage (V_{th}) was about -25 V with an on/off ratio of 5×10^4. The relatively high hole mobility may result from the effective overlap between the intermolecular phenyl groups, which would enhance carrier transport.[50,51] To compare the electronic property of single nanoribbon with that of single nanorod, we also conducted the FET measurement on a single nanorod. The results are not as good as that of a single nanoribbon, since the contact problem plays a prohibiting role in FET construction. The particular polygonal shape of the nanorod makes it difficult to form smooth and tight contact with the electrodes, resulting in degradation of device performance. The contact to nanoribbons is much better due to the flat and smooth surface of nanoribbon, giving a large contact area with the electrodes.

In addition, we investigated the photoluminescence (PL) properties of the as-prepared nanoribbons and nanorods. Figure 7 shows the nanoribbons and nanorods exhibit strong luminescence with three peaks centered at 420, 440, and 456 nm, respectively. Curve fitting reveals that the PL peaks of nanoribbons and nanorods have the same positions but slightly different intensity, which may be attributed to the fact that nanoribbons and nanorods have the same crystal structure but different growth directions.[24]

(50) Gao, Y.; Jiang, P.; Song, L.; Liu, L.; Yan, X.; Zhou, Z.; Lium, D.; Wang, J.; Yuan, H.; Zhang, Z.; Zhao, X.; Dou, X.; Zhou, W.; Wang, G.; Xie, S. *J. Phys. D: Appl. Phys.* **2005**, *38*, 1061.

(51) Peng, X.; Manna, L.; Yang, W.; Wickham, J.; Scher, E.; Kadavanich, A.; Alivisatos, A. P. *Nature* **2000**, *404*, 59.

Conclusion

DPA single-crystal nanorods and nanoribbons were controllably synthesized via a simple surfactant-assisted process. By tuning the solubility of DPA via varying the volume ratio of solvents, the shape of nanostructures gradually changed from nanoribbons to nanorods. A growth mechanism has been proposed. Crystal structure analysis and quantum mechanical calculations both support that the contact between the two phenyl groups attached at the opposite positions of the anthracene backbone forms effective intermolecular linking for 1-D crystal growth. A single-nanoribbon FET was fabricated to study the electronic properties of the nanoribbon, which showed a hole mobility of 0.16 cm^2 V^{-1} s^{-1}. The nanoribbons and nanorods have similar photoluminescent properties.

Acknowledgment. We thank Prof. Dong Cheng (Institute of Physics, Chinese Academy of Sciences) and Prof. Kang Zhenhui (Soochow University) for the help with XRD analysis. This work was supported by the Research Grants Council of Hong Kong SAR, China (Project No. N_CityU125/05), and the CityU Strategic Research Grants (7002075) from the City University of Hong Kong. X.H.Z. thanks the National Basic Research Program of China (973 Program) (Grants 2006CB33000 and 2007CB936000) and the National Natural Science Foundation of China (Grant 50825304).

Supporting Information Available: Size distribution of nanoribbons and nanorods; detailed index information about the crystal structure of DPA nanostructures; detailed experimental data for the preparation of DPA nanoribbons and nanorods; and SEM images of DPA nanostructures formed without assistance of any surfactant (PDF). This material is available free of charge via the Internet at http: //pubs.acs.org.

CM801896R